Error Probability Bounds for Nuclear Detection: Improving Accuracy through Controlled Mobility

Chetan D. Pahlajani [a], Jianxin Sun [b], Ioannis Poulakakis [b], Herbert G. Tanner [b]

[a] *Department of Mathematical Sciences, University of Delaware, Newark, DE 19716*

[b] *Department of Mechanical Engineering, University of Delaware, Newark, DE 19716*

Abstract

A collection of static and mobile radiation sensors is tasked with deciding, within a fixed time interval, whether a moving target carries radioactive material. Formally, this is a problem of detecting weak time-inhomogeneous Poisson signals (target radiation) concealed in another Poisson signal (naturally occurring background radiation). Each sensor locally processes its observations to form a likelihood ratio, which is transmitted once—at the end of the decision interval—to a fusion center. The latter combines the transmitted information to optimally (in the Neyman-Pearson sense) decide whether the measurements contain a radiation signal, or just noise. We provide a set of analytically derived upper bounds for the probabilities of false alarm and missed detection, which are used to design threshold tests without the need for computationally intensive Monte Carlo simulations. These analytical bounds couple the physical quantities of interest to facilitate planning the motion of the mobile sensors for minimizing the probability of missed detection. The network reconfigures itself in response to the target motion, to allow more accurate collective decisions within the given time interval. The approach is illustrated in numerical simulations, and its effectiveness demonstrated in experiments that emulate the statistics of nuclear emissions using a pulsed laser.

Key words: Nuclear detection, mobile sensor networks, inhomogeneous Poisson processes, Chernoff bounds

1 Introduction

This paper proposes a theoretical framework for network-based decision making, tailored to the problem of detecting nuclear material in transit within a given time interval, using a network of small and inexpensive static and mobile radiation sensors. This is an instance of a general problem of detecting a signal buried in noise, which is found for either single sensor or sensor network settings in a surprisingly rich application domain, from nuclear detection [39, 43] and optical communications [57], to radar [64] and acoustic [32] surveillance, to medical sensing [15] and neuroscience [24], to natural disaster early warning systems [17], and to high-energy experimental physics [12].

A network approach to deploying and managing data from radiation sensors can be one out of several layers in a comprehensive, integrative system for nuclear detection [5, 55]. The sensor of choice is a Geiger counter; larger and more sophisticated sensors (providing spectroscopy information), are prohibitively expensive to be deployed on a large scale [56], and too big to be mounted on mobile platforms. In addition, any active (e.g. X-ray) interrogation technology cannot be used to check vehicles that carry passengers or livestock [55].

A first challenge in detecting the presence of radioactive material with this type of sensors is that such a detector not only picks up the signal coming from the material, but also another one from ubiquitous cosmic and naturally occurring background radiation. From the sensor's perspective, the two signals are of identical nature and once superimposed, it is impossible to tell them apart. A second challenge relates to attenuation: although a kilogram of Highly Enriched Uranium (HEU) can emit as many as 4×10^7 gamma rays per second [5], shielding and attenuation [39] limit the effective detection range to a few feet, and require detection times that can range from minutes to hours [55]. In fact, a study performed on the radiation emitted by actual nuclear missiles [19] concluded that for the type of warheads containing HEU, the gamma ray emission just 25 cm away from the warhead casing is comparable to background. In a similar study [18], it was concluded that a nuclear cruise-missile is

Email addresses: chetan@math.udel.edu (Chetan D. Pahlajani), jxsun@udel.edu (Jianxin Sun), poulakas@udel.edu (Ioannis Poulakakis), btanner@udel.edu (Herbert G. Tanner).

practically undetectable by portable gamma-ray detectors at a distance of more than 5 meters. And although remote count-based detection with vehicle-mounted sensors is possible [18], the required sensor sensitivity and resolution is beyond that of common portable detectors which would most likely form the basis of a mobile sensor network. The problem is exacerbated when the source of the signal that needs to be detected is in motion. Not only does the stochastic process describing the signal become time-inhomogeneous from the detector's perspective [39], but the detector(s) only have a limited amount of time to make a decision before the potential target disappears from sight. They are called to detect within a small time interval a Poisson signal, buried inside another comparable Poisson signal.

Networks of spatially distributed sensors have been recognized as an important component of a multi-layered approach to nonproliferation, security and defense [5]. The potential of static sensor networks for the detection of stationary [7, 9, 49] or moving [39] radiation sources has been examined. In this context, the value of *sensor* mobility in nuclear measurement has recently been recognized [11, 31, 36], but the problem setup has been different from the one in this paper. Either sensor motion was random and the objective was network coverage [36], or detector motion was controlled and the objective was radiation mapping [10, 11], or sensor paths were predetermined [33], or the source was static [31, 51, 52].

In a general setting, detection is a decision problem between two alternative hypotheses (source plus background vs. background only) and a fair amount of literature in signal processing exists [2,13,23,25,47,59]. A likelihood ratio test (LRT) is a common approach, according to which a certain ratio computed based on collected sensor data is compared to a constant threshold; if this ratio is above the threshold, we decide that a source is present (else, we decide a source is absent). Nuclear emission is modeled as a Poisson process, and the approaches for detecting Poisson signals using networks of detectors, generally follow either a Bayesian [3,6,37,39] or a sequential formulation [14, 30]. [1] Typically, data collected at individual sensors is assumed to be independent identically distributed (i.i.d.) (a notable exception is [56]). Sequential Probability Ratio Test (SPRT) approaches [8, 27] are not comparable to the one presented here for the following reason. In the SPRT setting, data is typically collected until such time as a decision can be made with sufficient accuracy. In our setting, however, the data is only available over a fixed time interval (while the target is within sensing range), at the end of which a decision necessarily has to be made. Networked Bayesian formulations, on the other hand, tend to be computationally intensive to the point that current computing power would limit the scale of networks that can implement them in real-time, to single-digit network sizes [3]. Neyman-Pearson formulations [28, 62] can be alternative to Bayesian approaches, but have not yet been adapted to the case of time-inhomogeneous Poisson processes like the ones resulting from relative motion between sensor and source.

Sensor mobility changes the dynamics of nuclear measurement. We now understand how and why closing the distance between sensor and source affects the information content of the sensor measurement [39]: the signal-to-noise ratio scales with the inverse square of the distance. In this sense, bringing a small sensor closer to the source has an effect equivalent to that of using a much bigger sensor at a greater distance. Sensor mobility can be exploited [11,31,33,36] in the context of nuclear measurement, but it is not entirely clear what exact purpose it should serve. For example, in [31, 33] the variance of the assumed mean count rate at each spatial bin was taken as a performance measure, while [10, 51, 52] used various information-theoretic measures. Although these choices are intuitive, they may be considered equally arbitrary from the perspective of the decision maker. What is more, it is not always clear how the performance metric depends explicitly on sensor mobility, and how the latter can *optimally* be utilized.

This paper formulates the fixed-interval detection problem of a mobile source by a reconfigurable sensor network as an LRT developed within the Neyman-Pearson framework [42]. In such a test, two types of errors can occur: the first is to decide that a source is present when there is not, and this constitutes a false alarm; the second is to decide that there is nothing when in fact there is a source, which is a case of missed detection. The Neyman-Pearson test is designed to minimize the probability of missed detection for a given acceptable probability of false alarm. The contribution of the paper is in showing explicitly how the relative distance between sensor and source affects the error probabilities in a fixed-interval LRT, formulated for detecting weak, time-inhomogeneous Poisson processes buried in Poisson background noise. Since the error probabilities cannot be analytically computed, however, this hinders their use in a sensor motion optimization scheme that would aim directly at improving the accuracy of the LRT. The paper addresses this problem by deriving appropriate Chernoff bounds as proxies for these error probabilities, and utilizes an optimal (motion) control approach to steer the sensors, as well as to derive the optimal threshold values for the decision test, as a function of sensor and source trajectories. Chernoff bounds [16, 25, 40, 54] are used in robust detection for scalar Poisson processes with uncertain intensities in [23]. The bounds are also employed in performance evaluation of communications systems [38, 41, 46, 60]. Connections between Chernoff bounds and large deviations are explored in [4, 29, 53].

Section 2 recalls from [42] the (Neyman-Pearson) opti-

[1] Arguably, both have common theoretical underpinnings [28, 62].

mal decision rule for our problem of interest. Section 3 derives analytical probability bounds for the fixed-interval detection test, tightens them, and validates them by comparing them to estimates obtained through Monte Carlo simulations. Section 4 exposes the relation between the bounds and the threshold value for the LRT. In Section 5, bound derivation and threshold selection are integrated into an optimal control formulation, aiming at steering mobile sensors along paths that enable measurements which support more confident decisions regarding the presence or absence of a source. Section 6 illustrates the application of this method through experiments conducted using a device that emulates nuclear emission. Section 7 summarizies the main points in the approach and outlines the contributions.

2 Problem Description

The problem is set as follows. A network of k radiation sensors is deployed over a spatial region of interest with the objective of deciding whether a moving vehicle (target) carries a radioactive source. The network observes a time-inhomogeneous Poisson process and has to decide—at the end of a fixed time interval $[0, T]$—between two hypotheses, H_0 (absence of source) and H_1 (presence of source), regarding the statistics of the observed process. The optimal Neyman-Pearson test to decide between H_0 and H_1 involves comparing a global likelihood ratio L_T accumulated over the interval $[0, T]$ against a suitably chosen threshold $\gamma > 0$, deciding H_1 if $L_T \geq \gamma$, and H_0 otherwise.

Of particular importance in the present work is the relationship between *sensor mobility* and *decision-making accuracy*, the latter being reflected through the error probabilities. To determine how controlled mobility enhances the performance of decision making, we focus on two closely related questions. First, what is the quantitative dependence of the error probabilities on the problem parameters, including those related to motion, and second, how should the mobile sensors be steered to improve decision-making accuracy. The first question fits into the larger framework of performance analysis of detection systems and is difficult to answer exactly. In fact, it is extremely hard (if not impossible) to obtain closed-form expressions for error probabilities when assuming arbitrary relative motion between source and sensors. We therefore resort to Chernoff bound techniques to characterize the effect of mobility on decision accuracy. Then, we utilize the bounds to design optimal motion controllers so that decision accuracy is enhanced.

2.1 Probabilistic Setup and Detection

We start with a measurable space $(\Omega, \mathscr{F})$, supporting a k-dimensional vector of counting processes $\boldsymbol{N}_t = (N_t(1), \ldots, N_t(k))$, $t \in [0, T]$. For our problem, $N_t(i)$ represents the number of counts registered at sensor $i \in \{1, 2, \ldots, k\}$ up to (and including) time $t \in [0, T]$. The two hypotheses H_0 and H_1 regarding the state of the environment correspond to two distinct probability measures on $(\Omega, \mathscr{F})$. Hypothesis H_0 corresponds to a probability measure $\mathbb{P}_0$, with respect to which the $N_t(i)$, $1 \leq i \leq k$, are independent Poisson processes over $t \in [0, T]$ with intensities $\beta_i(t)$, respectively. Hypothesis H_1 corresponds to a probability measure $\mathbb{P}_1$, with respect to which the $N_t(i)$, $1 \leq i \leq k$, are independent Poisson processes over $t \in [0, T]$ with intensities $\beta_i(t) + \nu_i(t)$, respectively. The decision problem is thus one of identifying the correct probability measure ($\mathbb{P}_0$ versus $\mathbb{P}_1$) on $(\Omega, \mathscr{F})$, based on a realization of the k-dimensional process $\boldsymbol{N}_t = (N_t(1), \ldots, N_t(k))$. The following requirements are imposed on β_i and ν_i.

Assumption 1 *For $1 \leq i \leq k$, $\beta_i : [0, T] \to [\beta_{\mathsf{min}}, \beta_{\mathsf{max}}]$ is a bounded, continuous function with $0 < \beta_{\mathsf{min}} < \beta_{\mathsf{max}} < \infty$, β_{min}, β_{max} independent of $i \in \{1, 2, \ldots, k\}$.*

Assumption 2 *For $1 \leq i \leq k$, $\nu_i : [0, T] \to [\nu_{\mathsf{min}}, \nu_{\mathsf{max}}]$ is a bounded, continuous function with $0 < \nu_{\mathsf{min}} < \nu_{\mathsf{max}} < \infty$, ν_{min}, ν_{max} independent of $i \in \{1, 2, \ldots, k\}$.*

Let $(\mathscr{F}_t^{\boldsymbol{N}} : 0 \leq t \leq T)$ be the filtration generated by the process $\boldsymbol{N}_t$.[2] Then, for any event $A \in \mathscr{F}_t^{\boldsymbol{N}}$, an observer of the sample path $s \mapsto \boldsymbol{N}_s$, $0 \leq s \leq t$, knows at time t whether or not the event A has occurred. The σ-field $\mathscr{F}_T^{\boldsymbol{N}}$ thus represents the information generated by the totality of sensor observations up to $t = T$; to wit, the information on which the decision must be based.

A test for deciding between hypotheses H_0 and H_1 on the basis of $\mathscr{F}_T^{\boldsymbol{N}}$ observations can be thought of as a set $A_1 \in \mathscr{F}_T^{\boldsymbol{N}}$ with the following significance: if the outcome $\omega \in A_1$, decide H_1; if $\omega \in A_0 \triangleq \Omega \setminus A_1$, decide H_0. For a test $A_1 \in \mathscr{F}_T^{\boldsymbol{N}}$, two types of errors might occur. A "false alarm" occurs when the outcome $\omega \in A_1$ (i.e. decide H_1) while H_0 is the correct hypothesis. A "miss" occurs when $\omega \in \Omega \setminus A_1$ (i.e. decide H_0) while H_1 is the correct hypothesis. Clearly, the probability of false alarm is given by $\mathbb{P}_0(A_1)$, while the probability of a miss is given by $\mathbb{P}_1(\Omega \setminus A_1)$. Then, the probability of detection is given by $\mathbb{P}_1(A_1) = 1 - \mathbb{P}_1(\Omega \setminus A_1)$.

In the Neyman-Pearson framework, one is given an acceptable upper bound on the probability of false alarm $\alpha \in (0, 1)$, and the problem is to find an optimal test: a set $A_1^* \in \mathscr{F}_T^{\boldsymbol{N}}$ which maximizes the probability of detection over all tests whose probability of false alarm is less than or equal to α. The following result describes the optimal test. The underlying probabilistic setup is as described above.

Theorem 3 ([42]) *Consider a network with k sensors and a fusion center connected in a parallel configura-*

[2] Thus, for $t \in [0, T]$, $\mathscr{F}_t^{\boldsymbol{N}} = \sigma(\boldsymbol{N}_s : 0 \leq s \leq t)$ is the smallest σ-field on Ω with respect to which all the (k-dimensional) random variables $\boldsymbol{N}_s$, $0 \leq s \leq t$, are measurable.

tion.[3] *For $1 \le i \le k$, let $N_t(i)$, $t \in [0,T]$ denote the observation at sensor i over the time interval $[0,T]$ and let $(\tau_n(i) : n \ge 1)$ be the jump times of $N_t(i)$. Assume that at decision time T, sensor i transmits to the fusion center the statistic*

$$L_T(i) \triangleq \exp\left(-\int_0^T \nu_i(s)ds\right) \prod_{n=1}^{N_T(i)} \left(1 + \frac{\nu_i(\tau_n(i))}{\beta_i(\tau_n(i))}\right)$$

computed on the basis of its observation $t \mapsto N_t(i)$, $t \in [0,T]$. Then, the test $A_1^* = \{L_T \ge \gamma\}$ performed at the fusion center, with $L_T \triangleq \prod_{i=1}^k L_T(i)$ and $\gamma > 0$ satisfying $\mathbb{P}_0(L_T \ge \gamma) = \alpha$, is optimal for $\mathscr{F}_T^{\boldsymbol{N}}$-observations in the sense that for any $A_1 \in \mathscr{F}_T^{\boldsymbol{N}}$ with $\mathbb{P}_0(A_1) \le \alpha$, we have $\mathbb{P}_1(A_1^*) \ge \mathbb{P}_1(A_1)$.

Remark 4 *There may not exist a γ for every $\alpha \in (0,1)$.*[4] *The classical Neyman-Pearson result covers such cases by allowing tests with randomization [34, 45]. Randomization does not fit this problem well because in nuclear detection, α is in a certain order of magnitude, rather than a specific number (for instance, one might require that α be of order 10^{-4}). Therefore, we will assume in the sequel that we have the flexibility to first choose γ, with the provision that $\alpha = \mathbb{P}_0(L_T \ge \gamma)$ is of the right order of magnitude.*

Remark 5 *To avoid cases of singular detection [45], we assume that $\mathbb{P}_1$ is absolutely continuous with respect to $\mathbb{P}_0$, denoted $\mathbb{P}_1 \ll \mathbb{P}_0$, i.e. for any $A \in \mathscr{F}$ with $\mathbb{P}_0(A) = 0$, we have $\mathbb{P}_1(A) = 0$. In fact, given the probability measure $\mathbb{P}_0$, one can define $\mathbb{P}_1$ by the relation $d\mathbb{P}_1/d\mathbb{P}_0 = L_T$.*

2.2 Enhancing Decision Accuracy through Mobility

As stated earlier, the principal motivating application is reliable detection of moving nuclear material by networks of static and mobile sensors. Naturally, we would like a framework that allows for inclusion of inputs that control sensor motion. The discussion here and in Section 5 describes how such control inputs can be incorporated into our mathematical model, and justifies the validity of the results in this more general setting.

For simplicity, we focus on a planar scenario; note however that the proposed framework can be applied to accommodate three-dimensional configurations with minor modification. As noted, we have a network of k radiation sensors distributed in the (x,y)-plane with the objective of deciding whether a moving target vehicle carries a radioactive source. Sensors in the network can be static or mobile. Let $\boldsymbol{x}_i(t) \in \mathbb{R}^4$ be the value of the state vector at time $t \in [0,T]$ of sensor i, $1 \le i \le k$, which includes the location $(x_i(t), y_i(t)) \in \mathbb{R}^2$ of the sensor with respect to a reference frame and the corresponding velocity $(\dot{x}_i(t), \dot{y}_i(t)) \in \mathbb{R}^2$. If $\boldsymbol{x}(t) \in \mathbb{R}^{4k}$ denotes the augmented state at time t of the totality of sensors, the dynamics of the network can be written as

$$\dot{\boldsymbol{x}}(t) = \boldsymbol{f}(\boldsymbol{x}(t), \boldsymbol{u}(t)) \tag{1}$$

where $\boldsymbol{u}(t) \in \mathbb{R}^m$, for some $m \ge 1$, is the value of the control input at time t and $\boldsymbol{f} : \mathbb{R}^{4k} \times \mathbb{R}^m \to \mathbb{R}^{4k}$ is a vector field satisfying certain regularity conditions that guarantee the existence and uniqueness of solutions of (1) in the classical sense; in the context of the applications considered in this work, $\boldsymbol{f}$ is assumed to be smooth in $\boldsymbol{x}$ and $\boldsymbol{u}$. Finally, the following requirement is imposed on the class of admissible control inputs $\boldsymbol{u}$ that steer the motion of the mobile sensors.

Assumption 6 *The class $\mathscr{U}$ of admissible controls is contained in the space of bounded, piecewise-continuous functions $\boldsymbol{u} : [0,T] \to \mathbb{R}^m$, $m \ge 1$.*

Next, we examine how the introduction of dynamics (1) in the network affects the formulation of the detection problem of Section 2.1. First, note that if we allow for background activity that is spatially varying (assuming a radiation map is available) and possibly time varying, the intensity due to background at sensor i, denoted $\beta_i(t, \boldsymbol{u})$, will depend[5] on $\boldsymbol{u}$ through its dependence on the spatial location of sensor i. We suppose further that for each $\boldsymbol{u} \in \mathscr{U}$, the map $t \mapsto \beta_i(t, \boldsymbol{u})$ satisfies Assumption 1; this is certainly true if the background is spatially and temporally uniform, as in Section 5.

In the case where a radioactive source is present, the corresponding intensity is modeled as in [39]. In particular, if $(x_s(t), y_s(t))$ denotes the position at time t of a radioactive source of intensity $a > 0$, the intensity at sensor i is given by

$$\nu_i(t, \boldsymbol{u}) = \frac{\chi a}{\chi + r_i(t, \boldsymbol{u})^2}, \tag{2}$$

where χ is a sensor-specific cross-section coefficient and $r_i(t, \boldsymbol{u}) = [(x_s(t) - x_i(t))^2 + (y_s(t) - y_i(t))^2]^{1/2}$, the distance between the target vehicle and sensor i at time t. Again, the dependence of r_i on $\boldsymbol{u}$ is implicit, and it stems from the dependence of (x_i, y_i) on the input $\boldsymbol{u}$ through (1). Since $r_i(t, \boldsymbol{u})$ is necessarily a continuous function of t for each $\boldsymbol{u} \in \mathscr{U}$, and the map $r \mapsto \chi a/(\chi + r^2)$ is bounded, Assumption 2 holds.

[3] Thus, each sensor can only communicate with a central unit called the fusion center; see [58].

[4] If one were dealing instead with a *continuous* random variable Z admitting a density $f(x)$, one could always find γ by solving $\int_\gamma^\infty f(x)dx = \alpha$.

[5] The dependence of β_i on $\boldsymbol{u}$ is implicit, through the solution of (1). With a slight abuse of notation, $\boldsymbol{u}$ explicitly appears as an argument of β_i to emphasize the effect of the input on how the background intensity is perceived by a mobile sensor.

With these assumptions on the dynamics of the sensor motion, Theorem 3 applies with the likelihood ratio $L_T = L_T(\boldsymbol{u})$ obtained by replacing β_i, ν_i by $\beta_i(\cdot, \boldsymbol{u})$, $\nu_i(\cdot, \boldsymbol{u})$, respectively. Note that the probability measures $\mathbb{P}_0$ and $\mathbb{P}_1$ depend on $\boldsymbol{u}$. Indeed, for each $\boldsymbol{u} \in \mathscr{U}$, $\mathbb{P}_0^{\boldsymbol{u}}$ is a probability measure on $(\Omega, \mathscr{F})$ with respect to which the $N_t(i)$'s are independent Poisson processes with intensities $\beta_i(t, \boldsymbol{u})$. It follows from [42] that for each $\boldsymbol{u} \in \mathscr{U}$,

$$\frac{d\mathbb{P}_1^{\boldsymbol{u}}}{d\mathbb{P}_0^{\boldsymbol{u}}} = L_T(\boldsymbol{u}) \tag{3}$$

defines a probability measure $\mathbb{P}_1^{\boldsymbol{u}}$ on $(\Omega, \mathscr{F})$ with $\mathbb{P}_1^{\boldsymbol{u}} \ll \mathbb{P}_0^{\boldsymbol{u}}$ such that with respect to $\mathbb{P}_1^{\boldsymbol{u}}$, the $N_t(i)$'s are independent Poisson processes with intensities $\beta_i(t, \boldsymbol{u}) + \nu_i(t, \boldsymbol{u})$.

In order to exploit sensor mobility for greater decision accuracy, one would *ideally* like to find an optimal $\boldsymbol{u} \in \mathscr{U}$ which minimizes the probability of miss, subject to the constraint that the probability of false alarm not exceed some given $\alpha \in (0, 1)$. As noted earlier, however, the difficulty of finding closed-form expressions for the error probabilities seriously hinders this quest. As an alternative, we pose in Section 5 the following optimal control problem: Find $\boldsymbol{u} \in \mathscr{U}$ which minimizes the Chernoff upper bound on the probability of miss, while ensuring that the corresponding bound on the probability of false alarm does not exceed α.

Remark 7 *For notational convenience, we will drop the dependence on $\boldsymbol{u}$ in Sections 3 and 4 as we develop the bounds and related machinery, writing $\beta_i(t)$ for $\beta_i(t, \boldsymbol{u})$, $\nu_i(t)$ for $\nu_i(t, \boldsymbol{u})$, etc. As will be explained at the beginning of Section 5, the results of Sections 3 and 4 are valid for each fixed $\boldsymbol{u} \in \mathscr{U}$. The notational dependence on $\boldsymbol{u}$ will be revived in Section 5, when we optimize over $\boldsymbol{u}$. We also note that the calculations in Sections 3 and 4 are valid in a general detection setting which may not accommodate motion control of the sensors.*

3 Bounds on the Error Probabilities

The performance of the test $\{L_T \geq \gamma\}$ can be measured by the probabilities of false alarm and miss defined by

$$P_F \triangleq \mathbb{P}_0(L_T \geq \gamma) \qquad \text{and} \qquad P_M \triangleq \mathbb{P}_1(L_T < \gamma), \tag{4}$$

respectively. In many cases of interest, however, the exact computation of these error probabilities is mathematically intractable, motivating the need for good upper bounds which are easily computable. Theorem 8, stated below, derives such bounds on P_F and P_M using Chernoff's inequalities, and Proposition 13 provides conditions on achieving the tightest bounds for the test $\{L_T \geq \gamma\}$ given a threshold γ .

3.1 Chernoff Bounds

To state the main result of this section, we define, for $p \in \mathbb{R}$,

$$\Lambda(p) \triangleq \log \mathbb{E}_0[L_T^p] = \log \mathbb{E}_0[e^{p\,\ell_T}], \tag{5}$$

where $\ell_T \triangleq \log L_T$ is the log likelihood ratio, and $\mathbb{E}_i$ denotes expectation with respect to probability measure $\mathbb{P}_i$, $i \in \{0, 1\}$. $\Lambda(p)$ is thus the *cumulant generating function* of ℓ_T under H_0. Lemma 10 below assures us that $\Lambda(p)$ is well-defined for all $p \in \mathbb{R}$. We also let

$$\mu_i(t) \triangleq 1 + \frac{\nu_i(t)}{\beta_i(t)} \tag{6}$$

for $1 \leq i \leq k$, $t \in [0, T]$; thus, $\mu_i(t)$ is the ratio of intensities for H_1 versus H_0. The intensities at sensor i at time t under H_0 and H_1 can now be written as $\beta_i(t)$ and $\mu_i(t)\beta_i(t)$, respectively.

Theorem 8 *Let $\eta \triangleq \log \gamma \in \mathbb{R}$. The Chernoff bounds on P_F and P_M are given by*

$$\begin{aligned} P_F &\leq \exp\left(\inf_{p>0} \left[\Lambda(p) - p\eta\right]\right), \\ P_M &\leq \exp\left(\inf_{p<1} \left[\Lambda(p) + (1-p)\eta\right]\right), \end{aligned} \tag{7}$$

where for $p \in \mathbb{R}$, $\Lambda(p)$ is explicitly computable via

$$\Lambda(p) = \sum_{i=1}^{k} \int_0^T \left[\mu_i(s)^p - p\mu_i(s) + p - 1\right] \beta_i(s) ds \tag{8}$$

Before continuing with a proof of Theorem 8, it is remarked that the explicit analytical formula for $\Lambda(p)$ in (8) is a consequence of the assumption of deterministic intensities, which allows us to circumvent the intricate filtering analysis in [25] needed to accommodate stochastic intensities.

We prove Theorem 8 through a series of steps. The principal result in this direction is Proposition 9, stated next, whose application at $t = T$, in conjunction with (5), yields (8). To start, we introduce a stochastic process whose value at time T is the likelihood ratio L_T. Let $(L_t : t \in [0, T])$ be the process

$$L_t \triangleq \prod_{i=1}^{k} \left\{ \exp\left(\int_0^t [1 - \mu_i(s)]\beta_i(s) ds\right) \prod_{n=1}^{N_t(i)} \mu_i(\tau_n(i)) \right\},$$

with $\mu_i(t)$ given by (6). By convention, $\prod_{n=1}^{0}(\cdot) = 1$.

Proposition 9 *For any $p \in \mathbb{R}$, $t \in [0,T]$, we have*

$$\mathbb{E}_0[L_t^p] = \exp\left(\sum_{i=1}^{k} \int_0^t \left[\mu_i(s)^p - p\mu_i(s) + p - 1\right] \beta_i(s) ds\right).$$

Proposition 9 is proved using Lemmas 10 and 11 below, whose proofs are given in Appendix A.

Lemma 10 $\mathbb{E}_0[L_t^p] < \infty$ *for all* $p \in \mathbb{R}$, $t \in [0,T]$.

Lemma 11 *For any $p \in \mathbb{R}$, $t \in [0,T]$, we have*

$$L_t^p = 1 + \sum_{i=1}^{k} \int_0^t L_{s-}^p \left[\mu_i(s)^p - 1\right] dM_s(i) + \sum_{i=1}^{k} \int_0^t L_{s-}^p \left[\mu_i(s)^p - p\mu_i(s) + p - 1\right] \beta_i(s) ds \quad (9)$$

where $M_t(i) \triangleq N_t(i) - \int_0^t \beta_i(s) ds$.

Equipped with Lemmas 10 and 11, we provide

PROOF. [Proof of Proposition 9] Note that for each $1 \le i \le k$, $\int_0^t L_{s-}^p \left[\mu_i(s)^p - 1\right] dM_s(i)$ in (9) is a zero-mean $\mathbb{P}_0$-martingale by [2, Theorem II.3.T8]. Taking expectations in (9), we get

$$\mathbb{E}_0[L_t^p] = 1 + \int_0^t \mathbb{E}_0[L_{s-}^p] \left(\sum_{i=1}^{k} \left[\mu_i(s)^p - p\mu_i(s) + p - 1\right] \beta_i(s)\right) ds\,,$$

where we have used Lemma 10 to interchange integral and expectation. The stated result now follows from [2, Theorem A4.T4] with $x(t) = \mathbb{E}_0[L_t^p]$, $a(t) = t$, $u(t) = \sum_{i=1}^{k} \left[\mu_i(t)^p - p\mu_i(t) + p - 1\right] \beta_i(t)$.

To complete the proof of Theorem 8, we use a general fact about the LRT [25,40,45] stated in Lemma 12 below; see cited references for the proof.

Lemma 12 *For $\gamma > 0$, we have*

$$P_F \le \inf_{p>0} \left(\frac{1}{\gamma^p} \mathbb{E}_0[L_T^p]\right), \quad P_M \le \inf_{p<1} \left(\frac{1}{\gamma^{p-1}} \mathbb{E}_0[L_T^p]\right).$$

Finally, we have

PROOF. [Proof of Theorem 8] Writing $\mathbb{E}_0[L_T^p] = e^{\Lambda(p)}$, $\gamma = e^{\eta}$, Lemma 12 yields (7). Equation (8) is a direct consequence of (5) and Proposition 9 above.

3.2 Realizing the Probability Bounds

To effectively use Theorem 8, one needs to know where, if at all, the infima in (7) are realized. Moreover, for the bounds in (7) to be non-trivial, it is necessary that these infima be negative. Proposition 13 below assures us that if η is chosen to lie in the open interval $(\Lambda'(0), \Lambda'(1))$, where

$$\Lambda'(p) = \sum_{i=1}^{k} \int_0^T \left[\mu_i(s)^p \log \mu_i(s) - \mu_i(s) + 1\right] \beta_i(s) ds \quad (10)$$

and $\Lambda'(0) < 0 < \Lambda'(1)$, then there is a unique $p^* \in (0,1)$ satisfying $\Lambda'(p^*) = \eta$, for which both the infima in (7) are achieved and are negative.

To state Proposition 13, we introduce the functions $\mathscr{E}_F$, $\mathscr{E}_M$ mapping $(0,1)$ to $\mathbb{R}$ by

$$\mathscr{E}_F(p) \triangleq \Lambda(p) - p\,\Lambda'(p) \quad (11a)$$

$$\mathscr{E}_M(p) \triangleq \Lambda(p) + (1-p)\,\Lambda'(p). \quad (11b)$$

Proposition 13 *Fix $\eta = \log\gamma \in (\Lambda'(0), \Lambda'(1))$. Then, there is a unique $p^* \in (0,1)$ given by $\Lambda'(p^*) = \eta$ such that*

$$\inf_{p>0} \left[\Lambda(p) - p\eta\right] = \mathscr{E}_F(p^*) < 0, \qquad \inf_{p<1} \left[\Lambda(p) + (1-p)\eta\right] = \mathscr{E}_M(p^*) < 0. \quad (12)$$

The tightest error probability bounds for the decision test $\{L_T \ge \gamma\}$ are given by

$$P_F \le \exp[\mathscr{E}_F(p^*)], \quad P_M \le \exp[\mathscr{E}_M(p^*)]. \quad (13)$$

PROOF. We employ here a collection of Lemmas from Appendix B. Note that by Lemmas 16, 17, 18, $\Lambda'(\cdot)$ is continuous and strictly increasing with $\Lambda'(0) < 0 < \Lambda'(1)$. Hence, for any $\eta \in (\Lambda'(0), \Lambda'(1))$, there is a unique $p^* \in (0,1)$ with $\Lambda'(p^*) = \eta$. Since the C^2 functions $p \mapsto \Lambda(p) - p\eta$ and $p \mapsto \Lambda(p) + (1-p)\eta$ are also strictly convex by Lemma 17, they have unique global minima at p^*. Lemma 19 implies (12). Equation (13) follows from Theorem 8.

3.3 Error Probabilities: Bounds and Monte Carlo Estimates

To provide some indication regarding the ability of the bounds derived in Proposition 13 to capture the corresponding error probabilities, this section compares these bounds against Monte-Carlo estimates of P_F and P_M defined by (4). The comparison is performed in the context of the following example. Consider $k = 4$ identical

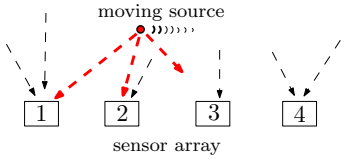

Fig. 1. A planar sensor array detecting a moving source. Thick dashed arrows mark gamma rays emitted by the source, while thin dashed arrows are background.

sensors (see Fig. 1) with cross-section coefficient [6] $\chi = 1$ $\mathtt{m}^2$. The sensors, stationary at planar coordinates (in $\mathtt{m}$) $(0,0)$, $(0.5,0)$, $(1.5,0)$, $(2.5,0)$, are labeled 1 through 4 respectively. A source of intensity $a = 2$ counts per second ($\mathtt{cps}$) is initialized at coordinates $(3.0, 0.5)$ $\mathtt{m}$, and starts moving parallel to the x axis, in a negative direction, from sensor 4 toward sensor 1, with a constant speed of 0.03 $\mathtt{m/s}$. The background is $\beta = 0.167$ $\mathtt{cps}$ and the decision time is $T = 100$ $\mathtt{s}$.

To generate samples of a nonhomogeneous Poisson process, we use the method of *thinning* [35, 44]. In more detail, to simulate a Poisson process with time-dependent intensity $\lambda(t)$, we first find a constant intensity $\lambda_d > 0$ which dominates $\lambda(t)$, i.e. $0 \le \lambda(t) \le \lambda_d$ for all $t \in [0,T]$. Assumptions 1 and 2 ensure that a suitable λ_d can be found. We next generate a sample path of a homogeneous Poisson process with intensity λ_d. Suppose that $T_1^*, T_2^*, \ldots, T_n^*$ are the event times (corresponding to jumps of the Poisson process) over $(0,T]$. Each event time T_j^* is retained with probability $\lambda(T_j^*)/\lambda_d$ and deleted with probability $1 - \lambda(T_j^*)/\lambda_d$. The retained event times now correspond to a sample path of a Poisson process with time-dependent intensity $\lambda(t)$ [35], [44, Theorem 3]. Notice that in our problem, $\lambda(t)$ will be of one of the two forms $\beta_i(t)$ and $\mu_i(t)\beta_i(t)$.

With this procedure at hand for generating samples of nonhomogeneous Poisson processes, we will estimate $P_F = \mathbb{P}_0(L_T \ge \gamma)$ and $P_M = \mathbb{P}_1(L_T < \gamma)$ for L_T computed as in Theorem 3 and for different values of the threshold $\gamma > 0$. To estimate the probability of false alarm P_F and the probability of miss P_M, let

$$A_\gamma \triangleq \{\omega \in \Omega : L_T(\omega) \ge \gamma\}$$
$$A_\gamma^c \triangleq \Omega \setminus A_\gamma = \{\omega \in \Omega : L_T(\omega) < \gamma\} \ .$$

We draw n samples $\omega_1, \omega_2, \ldots, \omega_n$ from Ω according to the probability measure $\mathbb{P}_0$, and n samples $\omega_1', \omega_2', \ldots, \omega_n'$ from Ω, now according to the probability measure $\mathbb{P}_1$. This corresponds to generating n realizations of the (k-dimensional) process $\boldsymbol{N}_t = (N_t(1), \ldots, N_t(k))$ over time $t \in [0,T]$, where the $N_t(i)$'s are independent Poisson processes with intensities given by β, and $\mu_i(t)\beta$, respectively. For each such realization, the likelihood ratios $L_T = L_T(\omega_i)$ and $L_T = L_T(\omega_i')$ can be computed as in Theorem 3. The probability of false alarm $P_F = \mathbb{P}_0(A_\gamma)$, and the probability of miss $P_M = \mathbb{P}_1(A_\gamma^c)$, can now be approximated by

$$P_F \approx \frac{1}{n}\sum_{i=1}^{n} 1_{A_\gamma}(\omega_i) \ , \quad P_M \approx \frac{1}{n}\sum_{i=1}^{n} 1_{A_\gamma^c}(\omega_i') \ . \quad (14)$$

To ensure that the estimates in (14) are sufficiently close to $\mathbb{P}_0(A_\gamma), \mathbb{P}_1(A_\gamma^c)$ with high enough probability, we need to choose n (number of samples) large enough. Indeed, for $\varepsilon, \delta \in (0,1)$, taking $n \ge \frac{1}{2\varepsilon^2} \ln \frac{2}{\delta}$ ensures [61] that the quantities in (14) estimate the corresponding probabilities to accuracy $\varepsilon > 0$ with confidence $1 - \delta$:

$$\mathbb{P}_0\left(\left|\frac{1}{n}\sum_{i=1}^{n} 1_{A_\gamma}(\omega_i) - \mathbb{P}_0(A_\gamma)\right| \le \varepsilon\right) \ge 1 - \delta \ ,$$
$$\mathbb{P}_1\left(\left|\frac{1}{n}\sum_{i=1}^{n} 1_{A_\gamma^c}(\omega_i') - \mathbb{P}_1(A_\gamma^c)\right| \le \varepsilon\right) \ge 1 - \delta \ .$$

For instance, to approximate the probabilities to within 1% (corresponding to $\varepsilon = 0.01$), with a confidence of 95% (corresponding to $\delta = 0.05$) we need 18 445 runs.

Figure 2 compares (the Monte Carlo estimates of) the error probabilities P_F and P_M with the corresponding Chernoff upper bounds, for various values of the threshold. Clearly, for both P_F and P_M, the Chernoff bounds and Monte Carlo estimates tend to agree around the values of 0 and 1 (the two ends of the horizontal axis). Due to the constraint imposed on the probability of false alarm (typically, far below 0.1), realistic instantiations of these bounds are more likely to occur at values of P_F close to zero, suggesting large thresholds, further to the right than the depicted scale in Fig. 2. Extrapolating from the graphs of the figure—which could not be easily extended to this part of the threshold domain, due to numerical difficulties in obtaining reasonable estimates using the Monte-Carlo method—indicates that the Chernoff bound for the probability of false alarm, maintaining its decreasing trend, will further close the distance between itself and the actual false alarm probability. For example, based on Fig. 2, and for an acceptable false alarm rate of less than 5%—still quite big—the error in approximating this probability using the Chernoff bound is in the order of 20%. But, what is more important in the context of sensor mobility optimization is the fact that the slopes of the curves of both bounds and Monte Carlo probability estimates are consistent, indicating that using the bounds as a proxy for the true—but unknown—error probabilities may not significantly affect the performance of optimal controllers.

[6] The values for these calculations are chosen to match the experimental parameters of Section 6; they are not to be understood in themselves as typical in a real nuclear detection scenario, although their relative scale can produce computational results that are—see [26].

4 Analytical Threshold Selection

This section discusses a procedure for selecting the threshold γ so that the LRT $\{L_T \geq \gamma\}$ conforms with desired performance requirements, typically characterized by the probability of false alarm P_F being less than or equal to a given level α. To avoid the complexity associated with obtaining closed-form expressions for the error probabilities, one may resort to numerical computations. This, however, presents at least two significant challenges. The first is the sizeable computational burden. Indeed, if one selects any particular γ, and uses a Monte Carlo method to estimate (say) P_F to an accuracy of 10^{-3} (not unreasonable, if the desired probability of false alarm is set at 10^{-2}) with 95% confidence, then at least $0.5 \times 10^6 \ln\left(\frac{2}{0.05}\right) \approx 1\,844\,439.73$ simulation runs will be required [61]. The second challenge is that numerical computations of the error probabilities as a function of threshold—as in Fig. 2, for example—are tied to a specific source motion and sensor configuration. Should any of the parameters change, the numerical computation has to be repeated.

In such instances, the Chernoff bounds derived in Proposition 13 provide a simple and elegant method for selecting the threshold $\eta = \log \gamma$, at the expense of some sharpness. The idea is to use the upper bounds on P_F and

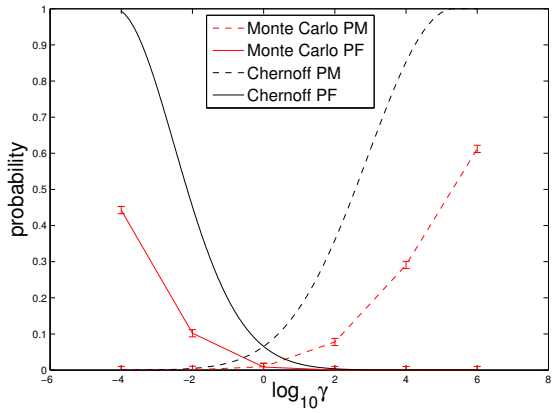

Fig. 2. Comparison between our Chernoff bounds and Monte Carlo simulation estimates of the error probabilities —false alarm (PF), and probability of miss (PM)—for a range of different likelihood ratio thresholds. The Monte Carlo probability estimates are shown in piecewise linear curves, while Chernoff bounds curves are smooth. Solid curves denote estimates on the probability of false alarm, and dashed curves correspond to probability of miss estimates. The 95% confidence intervals are marked over Monte Carlo estimate points. The emission rates for source and background are taken equal to the ones used in Section 6: $a = 2$ cps for the source, and $\beta = 0.167$ cps for background. These activity numbers may be artificial, selected to match our (slow) emission rates of our emulation apparatus of Section 6, but their ratio matches the order of magnitude of intensities in real-life detection scenarios [18].

P_M as proxies for the corresponding probabilities and formulate the problem as follows: Suppose $\alpha \in (0,1)$ is given. Knowing the tightest bounds on P_F, P_M for given η by (13), how should η be chosen to minimize the tightest upper bound on P_M while ensuring that the tightest upper bound on P_F does not exceed α? The identification of η is thus reduced to a tractable (deterministic) constrained optimization problem.

In more detail, Proposition 13 ensures that for every $\eta \in (\Lambda'(0), \Lambda'(1))$, there is a unique $p^* \in (0,1)$, satisfying $\Lambda'(p^*) = \eta$, where the tightest bounds on P_F, P_M for the LRT $\{L_T \geq e^\eta\}$ are attained. Since there is a one-to-one correspondence between $(0,1)$ and $(\Lambda'(0), \Lambda'(1))$ given by the strictly increasing continuous function $p \mapsto \Lambda'(p)$, one can pose the search for suitable $\eta \in (\Lambda'(0), \Lambda'(1))$ in terms of a search for suitable $p \in (0,1)$, with the understanding that for any $p \in (0,1)$, the corresponding η is given by $\eta = \Lambda'(p)$. Recalling (11a)–(11b), we have the constrained minimization problem

$$\text{Min } \mathscr{E}_M(p) \text{ over } p \in (0,1) \text{ with } \mathscr{E}_F(p) \leq \log \alpha \,. \quad (15)$$

Proposition 14, stated next, says that for sufficiently large α, there is a unique solution $p^\dagger \in (0,1)$ to (15).

Proposition 14 *Suppose* $\log \alpha > -\Lambda'(1)$. *There is a unique solution* $p^\dagger \in (0,1)$ *to the equation* $\mathscr{E}_F(p) = \log \alpha$. *This* $p^\dagger$ *minimizes* $\mathscr{E}_M(p)$ *over all* $p \in (0,1)$ *which satisfy* $\mathscr{E}_F(p) \leq \log \alpha$. *The minimum value of* $\mathscr{E}_M$ *is given by* $\mathscr{E}_M(p^\dagger) = \log \alpha + \Lambda'(p^\dagger)$. *For* $\eta = \Lambda'(p^\dagger)$, *i.e.,*

$$\gamma = e^{\Lambda'(p^\dagger)} \quad (16)$$

in the decision test $\{L_T \geq \gamma\}$, *we have*

$$P_F \leq \alpha \,, \qquad P_M \leq \alpha\, e^{\Lambda'(p^\dagger)} \,.$$

PROOF. Lemma 19 in Appendix B implies that on the interval $(0,1)$, $\mathscr{E}_F$ is strictly decreasing, while $\mathscr{E}_M$ is strictly increasing with

$$\inf_{p\in(0,1)} \mathscr{E}_F(p) = -\Lambda'(1) \,, \quad \sup_{p\in(0,1)} \mathscr{E}_F(p) = 0 \,,$$
$$\inf_{p\in(0,1)} \mathscr{E}_M(p) = \Lambda'(0) \,, \quad \sup_{p\in(0,1)} \mathscr{E}_M(p) = 0 \,.$$

Thus, in order that there exist $p \in (0,1)$ with $\mathscr{E}_F(p) \leq \log \alpha$, it is necessary (and sufficient) that α satisfy $\log \alpha > -\Lambda'(1)$. With this restriction in place, there is a unique $p^\dagger \in (0,1)$ with $\mathscr{E}_F(p^\dagger) = \log \alpha$, where we have used the fact that $\log \alpha < 0$. Since $\mathscr{E}_M$ is strictly increasing, we see that $p^\dagger$ is the unique solution to the constrained minimization problem (15). As discussed, η should be chosen to equal $\Lambda'(p^\dagger)$. The bounds on P_F, P_M follow from Theorem 8.

5 Optimal Control of Mobile Sensors

Controlled sensor mobility can be utilized to enhance the accuracy of detection with respect to that achieved in the static setting of Section 3.3. The framework developed above provides an analytically tractable way to design the motion of the mobile sensors so that the upper bound on the probability of a miss is minimized while the upper bound on the probability of false alarm is guaranteed to be smaller than a pre-specified desired level.

As described in Section 2.2, incorporating sensor dynamics (1) that depend on a control input $\boldsymbol{u} \in \mathscr{U}$ satisfying Assumption 6, renders the likelihood ratio (3) an (implicit) function of $\boldsymbol{u}$. Consequently, the LRT error probabilities, as well as the corresponding Chernoff bounds, depend on $\boldsymbol{u}$ as well. To see how this plays out analytically, observe that the error probabilities $P_F(\boldsymbol{u})$, $P_M(\boldsymbol{u})$ are given by (4), but with $L_T(\boldsymbol{u})$ in place of L_T. By Theorem 8, the Chernoff bounds on $P_F(\boldsymbol{u})$, $P_M(\boldsymbol{u})$ are given by (7), with the modification that $\Lambda(p)$—now denoted $\Lambda_{\boldsymbol{u}}(p)$—is obtained by replacing $\beta_i(\cdot)$ and $\mu_i(\cdot)$ in (8) with $\beta_i(\cdot,\boldsymbol{u})$ and $\mu_i(\cdot,\boldsymbol{u}) \triangleq 1+\nu_i(\cdot,\boldsymbol{u})/\beta_i(\cdot,\boldsymbol{u})$, where $\nu_i(\cdot,\boldsymbol{u})$ is computed using (2). The tightest bounds are still given by Proposition 13, but with the interval $(\Lambda'_{\boldsymbol{u}}(0), \Lambda'_{\boldsymbol{u}}(1))$ depending on $\boldsymbol{u}$. We use $\mathscr{E}_F(p,\boldsymbol{u})$ and $\mathscr{E}_M(p,\boldsymbol{u})$ for the quantities in (11a)–(11b).

Suppose now that $\alpha \in (0,1)$ is given, and that for each $\boldsymbol{u} \in \mathscr{U}$, $\log\alpha > -\Lambda'_{\boldsymbol{u}}(1)$. Then, Proposition 14 assures us that for each fixed $\boldsymbol{u} \in \mathscr{U}$, there is a unique $p^\dagger(\boldsymbol{u}) \in (0,1)$ which satisfies

$$\mathscr{E}_F(p^\dagger(\boldsymbol{u}),\boldsymbol{u}) = \log\alpha \ . \tag{17}$$

Moreover, $p^\dagger(\boldsymbol{u})$ minimizes $\mathscr{E}_M(p,\boldsymbol{u})$ over all $p \in (0,1)$ which satisfy $\mathscr{E}_F(p,\boldsymbol{u}) \le \log\alpha$. This minimum value of $\mathscr{E}_M$ is given by

$$\mathscr{E}_M(p^\dagger(\boldsymbol{u}),\boldsymbol{u}) = \log\alpha + \Lambda'_{\boldsymbol{u}}\big(p^\dagger(\boldsymbol{u})\big) \ . \tag{18}$$

Thus, using threshold $\gamma(\boldsymbol{u}) = e^{\eta(\boldsymbol{u})}$, where $\eta(\boldsymbol{u}) = \Lambda'_{\boldsymbol{u}}(p^\dagger(\boldsymbol{u}))$, we have $P_F(\boldsymbol{u}) \le \alpha$, $P_M(\boldsymbol{u}) \le \alpha\gamma(\boldsymbol{u})$ for every $\boldsymbol{u} \in \mathscr{U}$.

The above observation motivates the statement of the control design problem for the network dynamics (1) as an optimal control problem. The idea here is that the utilization of sensor mobility can potentially reduce the probability of decision error. The main challenge in directly doing so (without the aforementioned analysis) is that these error probabilities are impossible to compute analytically, and their explicit dependence on control is unknown. The results of Section 3 circumvent this problem by exposing the explicit dependence on control of specific bounds on these error probabilities. This explicit dependence allows us to formalize decision performance metrics in terms of the bounds, and optimize motion with respect to them.

In view of (18), therefore, an optimal control problem can now be stated as follows: Find $\boldsymbol{u}$ to minimize the cost $J(\boldsymbol{u}) \triangleq \mathscr{E}_M\big(p^\dagger(\boldsymbol{u}),\boldsymbol{u}\big) - \log\alpha = \Lambda'_{\boldsymbol{u}}\big(p^\dagger(\boldsymbol{u})\big)$, which is expressed analytically as

$$J(\boldsymbol{u}) = \sum_{i=1}^{k} \int_0^T [\mu_i(\boldsymbol{u})^{p^\dagger(\boldsymbol{u})} \log\mu_i(\boldsymbol{u}) - \mu_i(\boldsymbol{u}) + 1]\beta_i(s)ds \ ,$$

subject to the sensor dynamics and (17), with the latter now written as

$$\sum_{i=1}^{k} \int_0^T [p^\dagger(\boldsymbol{u})\mu_i(\boldsymbol{u})^{p^\dagger(\boldsymbol{u})} \log\mu_i(\boldsymbol{u}) - \mu_i(\boldsymbol{u})^{p^\dagger(\boldsymbol{u})} + 1]\beta_i(s)ds = -\log\alpha \ .$$

It is emphasized that the μ_i's in the equations above are also functions of time.

To see how sensor mobility can be exploited in this way, consider an example similar to that of Section 3.3, only now we have $k = 5$ sensors with 1 and 5 being mobile. The five sensors are originally at locations $(x_1,y_1) = (-3,0)$, $(x_2,y_2) = (-1,0)$, $(x_3,y_3) = (0,0)$, $(x_4,y_4) = (1,0)$, $(x_5,y_5) = (3,0)$. We set $\boldsymbol{x} = (x_1,y_1,x_2,y_2,\ldots,x_5,y_5)^\intercal$, with $\big(x_1(t),y_1(t)\big)$, $\big(x_5(t),y_5(t)\big)$ evolving according to the dynamics

$$\begin{aligned} \ddot{x}_1 &= u_1 \ , \quad \ddot{y}_1 = u_2 \\ \ddot{x}_5 &= u_3 \ , \quad \ddot{y}_5 = u_4 \end{aligned} \tag{19}$$

with initial conditions $\big(x_1(0),y_1(0)\big) = (-3,0)$, $\big(x_5(0),y_5(0)\big) = (3,0)$, and $\boldsymbol{u} = (u_1,\ldots,u_4)^\intercal$. We further assume that the velocity and acceleration of the mobile sensors are subject to the constraints

$$|\dot{x}_i| \le 1 \ , \qquad |\dot{y}_i| \le 1 \ , \qquad |u_i| \le 5 \ . \tag{20}$$

The target now follows a circular trajectory of radius $R = 0.5$ m centered at the point $(0,2)$, with maximum velocity $v_s^{\max} = 1.26$ m/s and maximum acceleration $a_s^{\max} = 3.16$ m/s^2:

$$x_s(t) = 0.5\cos\left(\frac{4\pi t}{5}\right), \ y_s(t) = 2 + 0.5\sin\left(\frac{4\pi t}{5}\right). \tag{21}$$

In this example, to emphasize the effectiveness of mobility in improving decision accuracy, we will reduce the ratio of source to background intensities by an order of magnitude compared to the value used in Sections 3.3 and 6; we will assume that the target is indeed a source of radiation with activity $a = 8$ cps, while background is at a level of $\beta = 13$ cps. The signal we are called to detect is now really buried in the noise. In addition, we

also reduce the length of the decision time interval from 100 to 10 seconds.

The optimal control laws $\boldsymbol{u}$ are numerically computed [1, 20–22, 48]. Figure 3 presents the closed-loop paths for the mobile sensors 1 and 5 under the influence of the optimal control $\boldsymbol{u}$. It is evident that, under the optimal control input $\boldsymbol{u}$, sensors 1 and 5 move so as to minimize their instantaneous distance from the target, but due to their velocity bounds they cannot follow exactly the target's circular path. This is also evident in Fig. 4, that shows the history of the horizontal speeds of sensor 1 and the target (the source). While the sensor's speed is confined in the $[-1, 1]$ interval, the target's speed periodically exceeds that limit, forcing the sensor to cut its circular reference path trying to keep up with the faster source. With sensors 1 and 5 chasing the target along paths generated by the optimal control $\boldsymbol{u}^*$, the optimal value for the optimization cost turns out to be $J^* = \mathscr{E}_M\big(p^\dagger(\boldsymbol{u}^*), \boldsymbol{u}^*\big) = -2.07$, with the probability of false alarm being constrained to remain below[7] $\alpha = 10^{-3}$. This amounts (see (18)) to having $\eta(\boldsymbol{u}^*) = -2.07$, yielding, according to Proposition 14, an upper bound on the probability of missed detection of 1.26×10^{-4}.

In this scenario, the sensors' controlled mobility offered them an order of magnitude improvement in their Signal-to-Noise Ratio (SNR). We compute this SNR using the expression $\frac{S}{\sqrt{S+B}}$, where S denotes the (estimated) integrated source count rate, and B is the integrated background count rate [39]. Had all sensors remained stationary during the 10 second time window, the SNR for detectors $1, \ldots, 5$ would have been 0.4980, 1.1434, 1.3617, 1.1434, and 0.4980, respectively. With sensors 1 and 5 chasing the target, they improve their SNR to 4.6843.

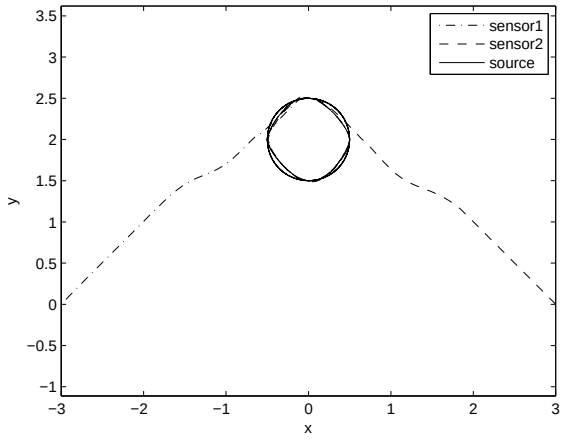

Fig. 3. Source path and optimal paths for mobile sensors 1 and 5. The source is circling at a radius of 0.5 around point (0,2), and is approached by sensor 1 from the left, and sensor 5 from the right. The two sensors cannot keep up with the source due to their motion constraints, so they "cut" the source's circular path along rounded inscribed rectangles.

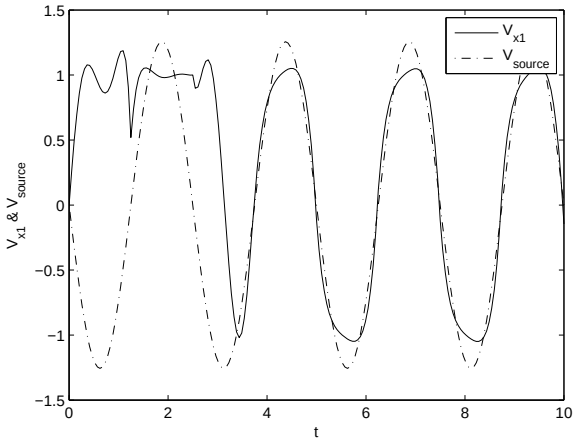

Fig. 4. Horizontal velocity of target (source) and sensor 1 over time. The sensor's absolute speed is upper bounded by 1, while the target's periodically exceeds that bound. The sensor cannot track the motion of the faster source perfectly.

6 Experimental Results in One Dimension

We validate the utility of the error probability bounds through experimentation with custom-built hardware that emulates radioactivity on the plane without imposing any health risks. In particular, we emulate the statistics of radioactive decay as perceived by a Geiger counter using a novel device that emits laser beams in random directions on a horizontal plane, triggered at random times that are exponentially distributed. Of course, nuclear emission is truly three-dimensional and a planar emulation system cannot fully and faithfully capture the nature of this phenomenon. It has been shown, however, that along a fixed plane of motion for the detector, the statistics of the events incident to the sensor can be adequately approximated. Details of the emulation device design and validation against real radiation measurements from a Geiger counter are documented elsewhere [26].

6.1 Experimental Setup

The experimental setting is shown in Fig. 5. In this setting, the laser device is mounted on top of the white round mobile robot, acting as a surrogate source of radiation. The sensors are realized via long rectangular boxes containing light detectors, configured to pick up a laser emission. There are four static sensors, arranged along the same line at the edge of the gray floor mat, and a single mobile sensor, mounted on top of a black square mobile robot, which is steered along a line paral-

[7] Approximate current nuisance alarm rate at U.S. border crossings is reported as 10^{-4} [63].

lel to that of the static sensors, and at the same distance with respect to the target.

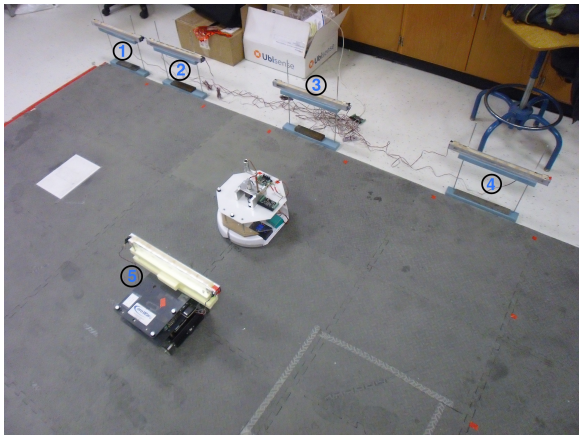

Fig. 5. The experimental setup that realizes a one dimensional detection scenario. In the static network tests, only sensors $1, \ldots, 4$ are used, while in the mobile network tests we utilize the spatial symmetry of the configuration to replace the static sensor 1 with the mobile sensor 5.

The stationary sensors $1, \ldots, 4$ are located at spatial coordinates $(0, 0)$, $(0.5, 0)$, $(1.5, 0)$, $(2.5, 0)$, respectively, with coordinates measured in $\mathtt{m}$. In Fig. 5, the leftmost sensor in the upper left corner is sensor 1. The mobile sensor, sensor 5, is initially at rest at location $(3, 1)$. The source is initialized at coordinates $(3.0, 0.5)$, and starts moving parallel to the x axis, in a negative direction, from sensor 4 toward sensor 1, with a constant speed of $0.03\ \mathtt{m/s}$. The source's intensity is a constant $a = 2\ \mathtt{cps}$, while the background rate is at $\beta = 0.167\ \mathtt{cps}$. The time interval for the detection is a window of $100\ \mathtt{s}$, and the acceptable probability of false alarm is set at $\alpha = 10^{-3}$.

Note that in the two dimensional setting of Fig. 5, the source intensity as perceived by a sensor is no longer inversely proportional to the square of the distance, as typically considered for the three-dimensional case [39]. Now the solid angle in χ scales linearly with the distance [26]; in both cases, the perceived intensity is in fact inversely proportional to the *solid angle* associated with the volume between the source and the sensor's surface. This solid angle scales with the square of the radius in three dimensions, but linearly on the plane. The perceived intensity ν is obtained as $\nu = \frac{a\phi}{2\pi}$. This intensity varies between $0.03\ \mathtt{cps}$ and $0.24\ \mathtt{cps}$, which is comparable to the background rate of $\beta = 0.167\ \mathtt{cps}$.

To simulate that uniform background rate—it cannot be reproduced by the laser device, for it would experience the same attenuation as the source signal—the count output of each sensor is superimposed externally with a temporal sequence of samples drawn from a Poisson distribution with mean β. We can thus know what percentage of the total average count rate is attributed to the source, but the detection algorithm is unaware of this; instead, it is presented with the count sum, and this is what it uses to compute the likelihood ratios.

6.2 Results and Discussion

To assess the contribution of mobility to the accuracy of detection, we run experiments for two cases: one in which the data collected from four static sensors $1, \ldots, 4$ are utilized to make a decision, and one in which static sensor 1 is replaced with the mobile sensor 5 so that the total number of sensors is constant and equal to four in both cases; see Fig. 5.

Thirty-two different runs are performed. For each run, finite-interval LRTs with a range of different threshold values, from 10^{-4} to 10^{6}, are conducted. The error probabilities for each threshold value are estimated as empirical averages over the set of all 32 LRTs conducted with that same threshold value.

Figure 6 compares the empirical average of the probability of miss for LRTs conducted over a range of different threshold values for 32 different experimental trials with 4 static sensors, against Monte Carlo estimates of this probability, and the proposed Chernoff bound. Figure 6 indicates that empirical averages from the experiments with the static network remain close to Monte Carlo estimates, suggesting an agreement between experimental and simulation results. In this context, the Chernoff bounds are shown to be tight in the region of low thresholds, while becoming more conservative for higher threshold values.

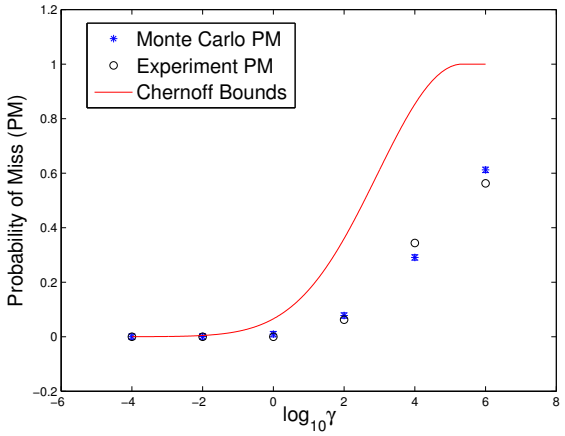

Fig. 6. Comparison between Chernoff bound, Monte Carlo and Experiment estimates for probability of miss in Case I when all sensors are static. The bars show the confidence interval of estimates of probabilities using both Monte Carlo and experimental data.

Table 1 lists the detection results over a set of the 32 static and mobile sensor network configuration trials, when the optimal controls $\boldsymbol{u}^*$, and optimal thresholds $\gamma(\boldsymbol{u}^*)$ are utilized. The third column in Table 1 lists the computed Chernoff bounds on the probability of missed

Table 1
Optimal LRT parameters, and detection results for the static and mobile sensor network configurations

network topology	optimal threshold	Chernoff bound	missed sources	empirical probability
static	540.70	0.541	4	0.125
mobile	27.98	0.028	0	–

detection, while the two rightmost columns document the frequency of missed detection errors. For the case of the mobile sensor, the resulting threshold is much smaller compared to that of the static case. The Chernoff bound on the probability of missed detection is lower than 3%, and agrees with experimental data where the source is detected in all 32 tests. In contrast, the static case Chernoff bound (54.1%) is conservative compared to the actual error probability results (12.5%), due to the inherent conservativeness of the bounds. Nonetheless, Table 2 that reports the SNR for the two cases computed using the same expression used in Section 5, suggests a clear three-fold improvement in the signal-to-noise ratio due to sensor mobility, corroborating the simulation results of Section 5.

Table 2
SNR of individual sensors in the experimental tests, for static and mobile sensor network configurations

network topology	SNR 1	SNR 2	SNR 3	SNR 4	SNR 5
static	**1.25**	1.79	2.03	1.78	–
mobile	–	1.79	2.03	1.78	**3.78**

7 Conclusions

This paper proposes a detection method for a network of mixed static and mobile sensors tasked with deciding whether a moving target carries a weakly emitting radioactive source. It is a problem of detecting a time-inhomogeneous Poisson process concealed in another Poisson process. Because of the analytical intractability of obtaining closed-form expressions for the error probabilities for the optimal likelihood ratio test, the paper suggests upper bounds for these quantities, which can subsequently be used to steer the mobile sensors along paths that enable more accurate network decisions. Explicit expressions for these bounds are derived in a form that incorporates the relative motion between the moving target and the mobile sensors, and are then used to facilitate the design of (sub)optimal control laws for the mobile sensors to significantly enhance the performance of decision making. The ability of the bounds to capture the underlying probabilities is discussed in detail through Monte Carlo simulations in the context of specific detection scenarios. Experiments in a planar setting using a device that emulates nuclear emission, demonstrate the benefits of using mobile sensors with suitably designed motion, and show a significant increase in detection performance.

Acknowledgements. The authors thank Ben Hockman for making the laser emulation device available and helping in the conduct of the experiments. This work was supported in part by ARL MAST CTA W911NF-08-2-0004.

A Proofs

PROOF. [Proof of Lemma 10] The result is obviously true for $p = 0$. Assume first that $p > 0$. Let $K_p \triangleq (1+\nu_{\mathsf{max}}/\beta_{\mathsf{min}})^p$. Recalling Assumptions 1 and 2, we have $L_t^p \le \prod_{i=1}^k K_p^{N_t(i)}$. Thus, $\mathbb{E}_0[L_t^p] \le \mathbb{E}_0\big[\prod_{i=1}^k K_p^{N_t(i)}\big] = \prod_{i=1}^k \mathbb{E}_0\big[K_p^{N_t(i)}\big]$, the latter equality following from independence. Since $N_t(i)$ is Poisson with intensity $\beta_i(t)$ under $\mathbb{P}_0$, we have $\mathbb{E}_0\big[K_p^{N_t(i)}\big] = \exp[(K_p-1)\int_0^t \beta_i(s)ds]$. Hence, $\mathbb{E}_0[L_t^p] \le \exp\big[(K_p-1)\sum_{i=1}^k \int_0^t \beta_i(s)ds\big] < \infty$. If $p < 0$, given $\prod_{n=1}^{N_t(i)} \big(1+\frac{\nu_i(\tau_n(i))}{\beta_i(\tau_n(i))}\big)^p \le 1$, we have $L_t^p \le \exp\big(-p\sum_{i=1}^k \int_0^t \nu_i(s)ds\big)$, implying that $\mathbb{E}_0[L_t^p] < \infty$.

PROOF. [Proof of Lemma 11] Note that the result is clearly true for $p = 0$. For $p \in \mathbb{R}\setminus\{0\}$, $t \in [0,T]$, we have

$$L_t^p = \exp\Big(p\sum_{i=1}^k \int_0^t [1-\mu_i(s)]\beta_i(s)ds\Big)\prod_{i=1}^k\prod_{n=1}^{N_t(i)} \mu_i(\tau_n(i))^p\,.$$

Let $x(t) \triangleq \prod_{i=1}^k\prod_{n=1}^{N_t(i)}[\mu_i(\tau_n(i))]^p$ and let $y(t) \triangleq \exp\Big\{p\sum_{i=1}^k \int_0^t [1-\mu_i(s)]\beta_i(s)ds\Big\}$, with the convention that $\prod_{n=1}^0(\dots) = 1$. For $t \in (0,T]$, $1 \le i \le k$, let $\Delta N_t(i) \triangleq N_t(i) - N_{t-}(i)$ be the jump in $N_t(i)$ at time t. Since $N_t(i)$ and $N_t(j)$ are independent for $i \ne j$, they have no common jumps (see Remark 15):

$$\sum_{0<t\le T} \Delta N_t(i)\cdot\Delta N_t(j) = 0, \qquad \mathbb{P}_0\text{-a.s.} \tag{A.1}$$

Hence, for $t \in (0,T]$,

$$x(t) = \begin{cases} x(t-)\cdot\mu_i(t)^p & \text{if } t = \tau_n(i),\ n \ge 1,\ 1 \le i \le k,\\ x(t-) & \text{else}\end{cases}$$

with $x(0) = 1$. Thus, $x(t)$ is right-continuous, monotone (non-decreasing if $p > 0$, non-increasing if $p < 0$) and piecewise constant with $\Delta x(t) \triangleq x(t) - x(t-)$ satisfying $\Delta x(t) = \sum_{i=1}^k \sum_{n\ge1} x(t-)\,[\mu_i(t)^p - 1]\,1_{(t=\tau_n(i))}$. Note also that $y(t)$ is differentiable with $y'(t) =$

$y(t) \cdot p\sum_{i=1}^{k}[1-\mu_i(t)]\beta_i(t)$. By the Product Formula [2, Theorem A4.T2], $x(t)y(t) = x(0)y(0) + \int_0^t x(s-)dy(s) + \int_0^t y(s)dx(s)$. If, for a stochastic process C_t, we define $\int_0^t C_s dN_s(i) \triangleq \sum_{n\geq 1} C_{\tau_n(i)} 1_{(\tau_n(i)\leq t)}$ for $t \in [0,T]$, $1 \leq i \leq k$, then it is easily seen that $\int_0^t y(s)dx(s) = \sum_{i=1}^{k} \int_0^t y(s)x(s-)\left[\mu_i(s)^p - 1\right] dN_s(i)$. Also, $\int_0^t x(s-)dy(s) = \int_0^t x(s-)y'(s)ds$, where y' is as given above. Noting that $y(s) = y(s-)$ for all $s \in [0,T]$ (owing to the continuity of $y(\cdot)$), we get $L_t^p = 1 + \sum_{i=1}^{k} \int_0^t L_{s-}^p \left[\mu_i(s)^p - 1\right] dN_s(i) + p\sum_{i=1}^{k} \int_0^t L_{s-}^p \left[1-\mu_i(s)\right] \beta_i(s)ds$. Since $M_t(i) = N_t(i) - \int_0^t \beta_i(s)ds$, we now get the stated result.

Remark 15 *The claim in* (A.1) *can be verified as follows. Let* $(\tilde{L}_t : t \in [0,T])$ *be the process* $\tilde{L}_t \triangleq \prod_{i=1}^{k} \left\{ \exp\left(\int_0^t [\beta_i(s) - 1]ds \right) \prod_{n=1}^{N_t(i)} \frac{1}{\beta_i(\tau_n(i))} \right\}$. *Since* $0 < \beta_{\mathsf{min}} \leq \beta_i(t) \leq \beta_{\mathsf{max}} < \infty$ *for all* $t \in [0,T]$, $1 \leq i \leq k$, *one can check that the equation* $d\mathbb{Q}/d\mathbb{P}_0 = \tilde{L}_T$ *defines a probability measure* $\mathbb{Q}$ *on* $(\Omega, \mathscr{F})$ *such that* $\mathbb{Q}$ *and* $\mathbb{P}_0$ *are mutually absolutely continuous*[8] *with* $d\mathbb{P}_0/d\mathbb{Q} = 1/\tilde{L}_T$. *Moreover, with respect to* $\mathbb{Q}$, *the* $N_t(i)$*'s are independent Poisson processes with intensity 1. Since, by [50, Proposition XII.1.5],* $\sum_{0<t\leq T} \Delta N_t(i) \cdot \Delta N_t(j) = 0$, $\mathbb{Q}$*-a.s., we must have* (A.1)*, owing to* $\mathbb{P}_0 \ll \mathbb{Q}$.

B Properties of $\Lambda(p)$

We establish here certain properties of $\Lambda(p)$ which play an important role in our analysis.

Lemma 16 *The function* $p \mapsto \Lambda(p)$ *is* C^2 *and*

$$\Lambda'(p) = \sum_{i=1}^{k} \int_0^T \left[\mu_i(s)^p \log \mu_i(s) - \mu_i(s) + 1\right] \beta_i(s)ds \ ,$$
$$\Lambda''(p) = \sum_{i=1}^{k} \int_0^T \mu_i(s)^p [\log \mu_i(s)]^2 \beta_i(s)ds \ .$$

PROOF. For each fixed $s \in [0,T]$, the integrand in (8) is smooth in p. From (6) and Assumptions 1, 2, it follows that one can take arbitrarily many derivatives of $\Lambda(p)$ with respect to p by simply differentiating under the integral sign.

Using the expression for $\Lambda''(p)$ in Lemma 16 and recalling (6) and Assumptions 1, 2, it follows that

Lemma 17 *For all* $p \in \mathbb{R}$, *we have* $\Lambda''(p) > 0$. *Consequently, the function* $p \mapsto \Lambda(p)$ *is strictly convex.*

[8] Thus, $\mathbb{Q}$ is absolutely continuous with respect to $\mathbb{P}_0$ (denoted $\mathbb{Q} \ll \mathbb{P}_0$) and $\mathbb{P}_0$ is absolutely continuous with respect to $\mathbb{Q}$ (denoted $\mathbb{P}_0 \ll \mathbb{Q}$).

Lemma 18 *We have* $\Lambda'(0) < 0$, $\Lambda'(1) > 0$.

PROOF. Since $e^{x-1} = 1 + (x-1) + \frac{(x-1)^2}{2!} + \frac{(x-1)^3}{3!} + \ldots$, we have $e^{x-1} > x$ for $x > 1$. Taking logarithms and rearranging, we get $\log x - x + 1 < 0$ for all $x > 1$. Recalling that $\mu_i(s) > 1$, $\beta_i(s) > 0$ for $0 \leq s \leq T$, $1 \leq i \leq k$, we set $p = 0$ in the expression for Λ' in Lemma 16 to get $\Lambda'(0) < 0$. Let $g(x) \triangleq x \log x - x + 1$. Noting that $g'(x) = \log x$ and $g(1) = 0$, we get $g(x) = \int_1^x \log y \ dy$ for $x > 1$. Thus, $g(x) > 0$ for $x > 1$. Setting $p = 1$ in the expression for Λ' in Lemma 16, we get $\Lambda'(1) > 0$.

Lemma 19 *The differentiable function* $\mathscr{E}_F : (0,1) \to \mathbb{R}$ *defined by* (11a) *is negative, strictly decreasing with*

$$\inf_{p\in(0,1)} \mathscr{E}_F(p) = -\Lambda'(1) \ , \quad \sup_{p\in(0,1)} \mathscr{E}_F(p) = 0 \ .$$

The differentiable function $\mathscr{E}_M : (0,1) \to \mathbb{R}$ *defined by* (11b) *is negative, strictly increasing with*

$$\inf_{p\in(0,1)} \mathscr{E}_M(p) = \Lambda'(0) \ , \quad \sup_{p\in(0,1)} \mathscr{E}_M(p) = 0 \ .$$

PROOF. Let's first prove that $\mathscr{E}_F$, $\mathscr{E}_M$ are in fact negative on $(0,1)$. Since Λ is strictly convex, we have $\Lambda(q) > \Lambda(p) + \Lambda'(p)(q-p)$ for all $p, q \in \mathbb{R}$ with $p \neq q$. Thus, for $p \in (0,1)$, taking $q = 0$ and $q = 1$, we get $\Lambda(p) - p\Lambda'(p) < \Lambda(0) = 0$ and $\Lambda(p) + (1-p)\,\Lambda'(p) < \Lambda(1) = 0$, respectively. Noting that $\mathscr{E}_F$, $\mathscr{E}_M$ are differentiable by Lemma 16, we directly compute that $\mathscr{E}_F'(p) = -p\,\Lambda''(p) < 0$ for $p \in (0,1)$, and $\mathscr{E}_M'(p) = (1-p)\,\Lambda''(p) > 0$ for $p \in (0,1)$. This proves that $\mathscr{E}_F$ is strictly decreasing on $(0,1)$, while $\mathscr{E}_M$ is strictly increasing on $(0,1)$. The claim now follows.

References

[1] David A. Benson, Geoffrey T. Huntington, Tom P. Thorvaldsen, and Anil V. Rao. Direct trajectory optimization and costate estimation via an orthogonal collocation method. *Journal of Guidance Control and Dynamics*, 29(6):1435–1440, 2006.

[2] Pierre Brémaud. *Point Processes and Queues.* Springer-Verlag, 1981.

[3] Sean M. Brennan, Angela M. Mielke, and David C. Torney. Radioactive source detection by sensor networks. *IEEE Transactions on Nuclear Science*, 52(3):813–819, 2005.

[4] James A. Bucklew and John S. Sadowsky. A contribution to the theory of Chernoff bounds. *IEEE Transactions on Information Theory*, 39(1):249–254, 1993.

[5] R.C. Byrd, J.M. Moss, W.C. Priedhorsky, C.A. Pura, G. W. Richter, K.J. Saeger, W.R. Scarlett, S.C. Scott, and R.L. Wagner Jr. Nuclear detection to prevent or defeat clandestine nuclear attack. *IEEE Sensors Journal*, 5(4):593–609, 2005.

[6] Jean-Francois Chamberland and Venugopal V. Veeravalli. Decentralized detection in sensor networks. *IEEE Transactions on Signal Processing*, 51(2):407–416, 2003.

[7] Mani Chandy, Concetta Pilotto, and Ryan McLean. Networked sensing systems for detecting people carrying radioactive material. In *International Conference on Networked Sensing Systems*, pages 148–155, 2008.

[8] J.-C. Chin, N.S.V. Rao, D.K.Y. Yau, M. Shankar, Y. Yang, J.C. Hou, S. Srivathsan, and S. Iyengar. Identification of low-level point radiation sources using a sensor network. *ACM Transactions on Sensor Networks*, 7(3), 2010.

[9] J.-C. Chin, D.K.Y. Yau, and N.S.V. Rao. Efficient and robust localization of multiple radiation sources in complex environments. In *International Conference on Distributed Computing Systems*, pages 780–789, 2011.

[10] R. A. Cortez, H. G. Tanner, R. Lumia, and C. T. Abdallah. Information surfing for radiation map building. *International Journal of Robotics and Automation*, 26(1):4–12, 2011.

[11] R.A. Cortez, X. Papageorgiou, H.G. Tanner, A.V. Klimenko, K.N. Borozdin, R. Lumia, and W.C. Priedhorsky. Smart radiation sensor management; radiation search and mapping using mobile robots. *IEEE Robotics & Automation Magazine*, 15(3):85–93, 2008.

[12] K. Cranmer and T. Plehn. Maximum significance at the LHC and higgs decays to muons. *The European Physical Journal C*, 51:415–420, 2007.

[13] Mark H. A. Davis and Elias Andreadakis. Exact and approximate filtering in signal detection: An example. *IEEE Transactions on Information Theory*, 23(6):768–772, 1977.

[14] James DeLucia and H. Vincent Poor. Performance analysis of sequential tests between poisson processes. *IEEE Transactions on Information Theory*, 43(1):221–238, 1997.

[15] C. Estes, A. Duncan, B. Wade, C. Lloyd, W. Ellis Jr., and L. Powers. Reagentless detection of microorganisms by intrinsic fluorescence. *Biosensors and Bioelectronics*, 18:511–519, 2003.

[16] James E. Evans. Chernoff bounds on the error probability for the detection of non-Gaussian signals. *IEEE Transactions on Information Theory*, 20(5):569–577, 1974.

[17] M. Faulkner, M. Olson, R. Chandy, J. Krause, K.M Chandy, and A. Krause. The next big one: Detecting earthquakes and other rare events from community-based sensors. In *International Conference on Information Processing and Sensor Networks*, pages 13–24, 2011.

[18] S. Fetter, T.M. Cochran, L. Grodzins, H.L. Lynch, and M.S. Zucker. Gamma-ray measurements of a soviet cruise-missile warhead. *Science*, 248:828–834, 1990.

[19] S. Fetter, V.A¿ Frolov, M. Miller, R. Mozley, O.F. Prilutsky, S.N. Rodionov, and R.Z. Sagdeev. Detecting nuclear warheads. *Science & Global Security*, 1:225–302, 1990.

[20] Divya Garg, William W. Hager, and Anil V. Rao. Pseudospectral methods for solving infinite-horizon optimal control problems. *Automatica*, 47(4):829 – 837, 2011.

[21] Divya Garg, Michael Patterson, Camila Francolin, Christopher Darby, Geoffrey Huntington, William Hager, and Anil Rao. Direct trajectory optimization and costate estimation of finite-horizon and infinite-horizon optimal control problems using a Radau pseudospectral method. *Computational Optimization and Applications*, 49(2):335–358, 2011.

[22] Divya Garg, Michael Patterson, William W. Hager, Anil V. Rao, David A. Benson, and Geoffrey T. Huntington. A unified framework for the numerical solution of optimal control problems using pseudospectral methods. *Automatica*, 46(11):1843 – 1851, 2010.

[23] Evaggelos A. Geraniotis and H. Vincent Poor. Minimax discrimination for observed Poisson processes with uncertain rate functions. *IEEE Transactions on Information Theory*, 31(5):660–669, 1985.

[24] Joshua I. Gold and Michael N. Shadlen. The neural basis of decision making. *Annual Review of Neuroscience*, 30:535–574, 2007.

[25] Joseph L. Hibey, Donald L. Snyder, and Jan H. van Schuppen. Error-probability bounds for continuous-time decision problems. *IEEE Transactions on Information Theory*, 24(5):608–622, 1978.

[26] Benjamin J. Hockman, Jianxin Sun, and Herbert G. Tanner. Emulating nuclear emissions with a pulsed laser. *IEEE Transactions on Automation Science and Engineering*, 2012 (in print).

[27] K.D. Jarman, L.E. Smith, and D.K. Carlson. Sequential probability ratio test for long-term radiation monitoring. *IEEE Transactions on Nuclear Science*, 51(4):1662–1666, 2004.

[28] Thomas Kailath and H. Vincent Poor. Detection of stochastic processes. *IEEE Transactions on Information Theory*, 44(6):2230–2259, 1998.

[29] Dimitri Kazakos. Asymptotic error probability expressions for multihypothesis testing using multisensor data. *IEEE Transactions on Systems, Man and Cybernetics*, 21(5):1101–1114, September/October 1991.

[30] Dimitri Kazakos and P. Papantoni-Kazakos. Sequential detection between poisson processes. *IEEE Transactions on Information Theory*, 26(1):116–120, 1980.

[31] A.V. Klimenko, W.C. Priedhorsky, H. Tanner, K.N. Borozdin, and N. Hengartner. Intelligent sensor management in nuclear searches and radiological surveys. In *Transactions of the American Nuclear Society*, pages 21–22. 2006.

[32] Chris Kreucher and Ben Shapo. Multitarget detection and tracking using multisensor passive acoustic data. *IEEE Journal of Oceanic Engineering*, 36(2):205–218, 2011.

[33] Amit Kumar, Herbert G. Tanner, Alexei V. Klimenko, Konstantin Borozdin, and William C. Priedhorsky. Automated sequential search for weak radiation sources. In *Proceedings of the IEEE Mediterranean Conference on Control and Automation*, pages 1–6, June 2006.

[34] E. L. Lehmann. *Testing Statistical Hypotheses*. John Wiley & Sons, second edition, 1986.

[35] P. A. W Lewis and G. S. Shedler. Simulation of nonhomogeneous Poisson processes by thinning. *Naval Research Logistics Naval Research Logistics Quarterly*, 26(3):403–413, 1979.

[36] C.Y.T. Ma, D.K.Y. Yau, N.K. Yip, N.S.V. Rao, and J. Chen. Performance analysis of stochastic network coverage with limited mobility. In *IEEE International Conference on Mobile AdHoc and Sensor Systems*, pages 496–505, 2009.

[37] M. Morelande, B. Ristic, and A. Gunatilaka. Detection and parameter estimation of multiple radioactive sources. In *Proceedings of the International Conference on Information Fusion*, pages 1–7. IEEE, 2007.

[38] Laurie B. Nelson and H. Vincent Poor. Performance of multiuser detection for optical CDMA–Part I: Error Probabilities. *IEEE Transactions on Communications*, 43(11):2803–2811, 1995.

[39] Robert J. Nemzek, Jared S. Dreicer, David C. Torney, and Tony T. Warnock. Distributed sensor networks for detection of mobile radioactive sources. *IEEE Transactions on Nuclear Science*, 51(4):1693–1700, 2004.

[40] C. M. Newman and B. W. Stuck. Chernoff bounds for discriminating between two Markov processes. *Stochastics*, 2:139–153, 1979.

[41] John J. O'Reilly and Jose R. F. da Rocha. Improved error probability evaluation methods for direct detection optical communication systems. *IEEE Transactions on Information Theory*, 33(6):839–848, 1987.

[42] Chetan D. Pahlajani, Ioannis Poulakakis, and Herbert G. Tanner. Networked decision making for Poisson processes and application to nuclear detection. *IEEE Transactions on Automatic Control*, page (to appear).

[43] Chetan D. Pahlajani, Ioannis Poulakakis, and Herbert G. Tanner. Decision making in sensor networks observing poisson processes. In *IEEE Mediterranean Conference on Control and Automation*, pages 1230–1235, 2013.

[44] Raghu Pasupathy. Generating nonhomogeneous Poisson processes. In *Wiley Encyclopedia of Operations Research and Management Science*. Wiley, 2009.

[45] H. Vincent Poor. *An Introduction to Signal Detection and Estimation*. Springer-Verlag, second edition, 1994.

[46] Vasant K. Prabhu. Modified Chernoff bounds for PAM systems with noise and interference. *IEEE Transactions on Information Theory*, 28(1):95–100, 1982.

[47] P. Varaiya R. Boel and E. Wong. Martingales on jump processes II: Applications. *SIAM Journal on Control*, 13(5):1022–1061, 1975.

[48] Anil V. Rao, David A. Benson, Christopher Darby, Michael A. Patterson, Camila Francolin, Ilyssa Sanders, and Geoffrey T. Huntington. Algorithm 902: GPOPS, a MATLAB software for solving multiple-phase optimal control problems using the gauss pseudospectral method. *ACM Transactions on Mathematical Software*, 37(2):22:1–22:39, April 2010.

[49] N.S.V. Rao, J.-C. Chin, D.K.Y. Yau, C.Y.T. Ma, and R.N. Madan. Cyber-physical trade-offs in distributed detection networks. In *IEEE Conference on Multisensor Fusion and Integration for Intelligent Systems*, pages 88–95, 2010.

[50] Daniel Revuz and Marc Yor. *Continuous Martingales and Brownian Motion*. Springer, third edition, 1999.

[51] Branko Ristic and Ajith Gunatilaka. Information driven localisation of a radiological point source. *Information fusion*, 9(2):317—326, 2008.

[52] Branko Ristic, Mark Morelande, and Ajith Gunatilaka. Information driven search for point sources of gamma radiation. *Signal Processing*, 90(4):1225—1239, 2010.

[53] John S. Sadowsky. An asymptotically least-favorable Chernoff bound for a large class of dependent data processes. *IEEE Transactions on Information Theory*, 33(1):52–61, January 1987.

[54] Donald L. Snyder. *Random Point Processes*. Wiley-Interscience, 1975.

[55] Devabhaktuni Srikrishna, A. Narasimha Chari, and Thomas Tisch. Deterance of nuclear terrorism with mobile radiation detectors. *The Nonproliferation Review*, 12(3):573–614, 2005.

[56] Ashok Sundaresan, Pramod K. Varshney, and Nageswara S. V. Rao. Distributed detection of a nuclear radioactive source using fusion of correlated decisions. In *Proceedings of the International Conference on Information Fusion*, pages 1–7. IEEE, 2007.

[57] M.C. Teich and S. Rosenberg. Photocounting array receivers for optical communication through the lognormal atmospheric channel: optimum an dsuboptimum receiver structures. *Journal of Applied Optics*, 12:2616–2623, 1973.

[58] Pramod K. Varshney. *Distributed Detection and Data Fusion*. Springer-Verlag, 1997.

[59] Sergio Verdú. Asymptotic error probability of binary hypothesis testing for poisson point-process observations. *IEEE Transactions on Information Theory*, 32(1):113–115, 1986.

[60] Sergio Verdú. Multiple-access channels with point-process observations: Optimum demodulation. *IEEE Transactions on Information Theory*, 32(5):642–651, 1986.

[61] M. Vidyasagar. Statistical learning theory and randomized algorithms for control. *IEEE Control Systems Magazine*, 18(6):69–85, 1998.

[62] Ramanarayanan Viswanathan and Pramod K. Varshney. Distributed detection with multiple sensors: Part I - Fundamentals. *Proceedings of the IEEE*, 85(1):54–63, 1997.

[63] L.M. Wein and M.P. Atkinson. The last line of defense: designing radiation detection-interdiction systems to protect cities form a nuclear terrorist attack. *IEEE Transactions on Nuclear Science*, 54(3):654–669, 2007.

[64] Y. Yang, R.S. Blum, and B.M. Sadler. Energy-efficient routing for signal detection in wireless sensor networks. *IEEE Transactions on Signal Processing*, 57(6):2050–2063, 2009.